Composite Structures 305 (2023) 116473

Contents lists available at ScienceDirect

Composite Structures

journal homepage: www.elsevier.com/locate/compstruct

Sensitivity analysis and genetic algorithm-based shear capacity model for basalt FRC one-way slabs reinforced with BFRP bars

Abathar Al-Hamrani, Tadesse G. Wakjira, Wael Alnahhal *, Usama Ebead

Department of Civil and Architectural Engineering, College of Engineering, Qatar University, Qatar

ARTICLE INFO

Keywords:
BFRP bars
Basalt macro-fibers
Shear capacity
Genetic algorithms
Finite element model
Sensitivity analysis

ABSTRACT

Fiber-reinforced polymer (FRP) composites are increasingly used in concrete structures owing to their superior corrosion resistance. However, FRP-reinforced concrete (RC) structures exhibit less ductile response compared to steel RC structures. Recently, the use of basalt fiber reinforced concrete (BFRC) reinforced with BFRP bars was investigated to achieve a reasonable level of ductility in BFRC-BFRP one-way slabs. The shear behavior of such a slab depends on different design parameters. This paper aims to identify the impact of each design parameter on the shear behavior of BFRC-BFRP one-way slabs using a fractional factorial design of experiment (DOE). A 3D finite element model was first developed and validated against available experimental results. The developed model is then used to conduct a sensitivity analysis considering five factors that influence the shear behavior of BFRC-BFRP one-way slabs. These factors are the longitudinal reinforcement ratio, shear span-to-depth ratio, effective depth, concrete compressive strength, and volume fraction of basalt macro fibers (BMF). Finally, a design equation that can predict the shear capacity of one-way BFRC-BFRP slabs was proposed based on genetic algorithm. The proposed model showed the best prediction accuracy compared to the available design codes and guidelines with a mean of predicted to experimental shear capacities (V_{pred}/V_{exp}) ratio of 0.97 and a coefficient of variation of 17.91%.

1. Introduction

Nowadays, fiber-reinforced polymer (FRP) bars are attracting considerable interest in the construction industry and research as a sustainable alternative to conventional steel bars. FRP bars have remarkable features such as having 3 to 5 times higher ultimate tensile strength than steel bars, excellent corrosion resistance, high strength-to-weight ratio, and high flexibility with ease in handling [1,2]. Despite these outstanding features, FRP bars have shown some drawbacks including their higher initial cost compared to conventional steel bars, lower elastic modulus, and brittle behavior at failure [1,2]. Traditionally, carbon FRP (CFRP) [3] and glass FRP (GFRP) [4] are the most common types of FRP bars implemented in RC structures. Lately, basalt FRP (BFRP) bars have been attracting considerable interest due to their comparable mechanical and chemical properties to that of GFRP bars [5–7] and substantially better cost efficiency than CFRP bars [8]. However, their application for reinforcing one-way RC slabs is scarce [9–11] compared to that of other types of FRP bars [12–19]. Moreover, the existing studies primarily focused on studying the flexural behavior of one-way RC slabs reinforced with BFRP bars [9–11], while studies are still lacking concerning their shear behavior.

The shear behavior of FRP reinforced concrete one-way slabs is influenced by different parameters. El-Sayed et al. [12] have investigated the influence of reinforcement ratio (ρ_{frpl}) on the shear strength of CFRP and GFRP reinforced one-way slabs. Their test results revealed 20% and 36% increase in the shear capacity when the reinforcement ratio of CFRP bars was increased from 0.39% to 0.78% and from 0.78% to 1.18%, respectively. Similarly, increasing the ρ_{frpl} of GFRP bars from 0.86% to 1.7% has significantly increased the shear capacity by 26% [12]. Besides, the study by Abdulsalam et al. [19] indicated a 32% increase in the shear capacity of CFRP reinforced slab by increasing the ρ_{frpl} from 0.52% to 0.83% . Furthermore, the increase in compressive strength from 52 MPa to 76 MPa has increased the shear capacity from 159 kN to 168 kN.

While the concrete compressive strength is an essential factor that influences the shear capacity of RC sections, the concrete tensile strength represents another essential factor. However, the concrete is known to be weak under tension and has a brittle nature at failure.

* Corresponding author.
E-mail address: wael.alnahhal@qu.edu.qa (W. Alnahhal).

https://doi.org/10.1016/j.compstruct.2022.116473
Received 29 August 2022; Received in revised form 10 November 2022; Accepted 14 November 2022
Available online 17 November 2022

Therefore, adding macro fibers has been considered an effective way to enhance the concrete tensile strength and restrict crack widening [20]. High et al. [21] and Bajaj [22] reported that when basalt fibers were added to the concrete mix, thinner cracks were observed. As a consequence, the concrete material is expected to be less permeable with an enhanced fatigue strength and impact resistance [21]. A recent study by Alnahhal et al. [23] showed that the mechanical properties of concrete were considerably improved with increasing the volume fraction of basalt macro fibers. Moreover, while plain concrete has insignificant post-cracking tensile resistance, an additional tensile resistance will be provided by the fibers, which would have a remarkable benefit to the shear behavior of one-way RC slabs reinforced with FRP bars against the major diagonal shear cracks. Krassowska et al. [24] showed a 36% increase in the shear strength of basalt fiber reinforced concrete (BFRC) beams over that made with plain concrete. Recently, Al-Hamrani and Alnahhal [25] experimentally studied the effect of volume fraction (V_f) of basalt macro fibers (BMF) and the longitudinal reinforcement ratio on the shear behavior of BFRC-BFRP one-way slabs longitudinally reinforced with BFRP bars. Based on the experimental results, a 25–29% increase in the shear capacity was reported due to an increase of the reinforcement ratio from 0.792% to 1.27%. Additionally, the inclusion of BMF enhanced the shear strength by 4% to 16.7% and showed less brittle failure due to the bridging effect of fibers across the major shear crack.

Research on the shear behavior of FRP-RC one-way slabs has been mostly restricted to a limited number of studies, whereas a detailed investigation that covers the effect of different parameters on the shear behavior is recommended to enrich this research area. More attention must be given to this subject, particularly in light of the lower elastic modulus of FRP bars and their brittle nature, which are responsible for the reduction in several shear-resisting mechanisms of FRP-RC sections [26–28]. Moreover, despite the comparable mechanical and chemical properties of BFRP bars to that of GFRP bars, previous studies on FRP-RC one-way slabs have not investigated their shear behavior using BFRP bars as the main reinforcement. Furthermore, while previous studies reported that incorporating macro fibers in concrete has improved the mechanical properties of concrete, the research on the shear behavior of one-way FRP-RC slabs to date has focused only on the use of plain concrete slabs. Therefore, this paper is aimed to expand on the experimental work of Al-Hamrani and Alnahhal [25] by developing virtual experiments using the finite element method (FEM) to supplement the experimental work and further investigate the main and interaction effects of different design factors and propose a simple shear design equation. For this purpose, a sensitivity analysis was conducted using a three-level fractional factorial design of experiment (DOE) to investigate the main and two-way interaction effects of different key design parameters on the shear response of BFRC-BFRP one-way slabs. The main parameters considered in this study include the longitudinal reinforcement ratio (ρ_{frpl}), the shear span-to-depth (a/d) ratio, the effective depth (d) of slabs, the compressive strength ($f_{cf}^{'}$), and the volume fractions of basalt macro fibers. As a result, this study can provide an important opportunity to advance the understanding of the influence of different parameters and their interactions on the shear behavior of one-way BFRC-BFRP slabs. Finally, a genetic algorithm (GA) was used to propose a simple shear design equation for one-way BFRC-BFRP slabs that is believed to be beneficial to practitioners.

2. Model validation

2.1. FE model definition

Concrete is categorized as a quasi-brittle material that demonstrates a non-linear constitutive model caused mainly by the damage and plasticity process. The damage mechanism can be characterized by microcracking, while the plasticity behavior is attributed to the strain-softening, progressive deterioration, and volumetric expansion phenomenon [29–31]. Therefore, to accurately capture the non-linear response of concrete, the dynamic explicit method was used, and the concrete damaged plasticity (CDP) model was adopted in the analysis.

The compression crushing and tension cracking of concrete are the two failure mechanisms assumed in the CDP model. The values of the compression damage parameter (d_c) and the tensile damage parameter (d_t) range from 0 to 1. A value of 1 indicates a fully damaged material with a total loss of strength, while a value of 0 indicates a pristine material with no damage. In this study, the compression damage parameter is determined based on Eq. (1) below:

$$d_c = 1 - \frac{f_{cf}\ E_o^{-1}}{\varepsilon_{cf}^{pl}\left(\frac{1}{b_c} - 1\right) + f_{cf}\ E_o^{-1}} \tag{1}$$

$$\varepsilon_{cf}^{pl} = b_c \varepsilon_{cf}^{in} \tag{1a}$$

$$\varepsilon_{cf}^{in} = \varepsilon_{cf} - f_{c0} E_o^{-1} \tag{1b}$$

where f_{cf} represents the compressive stress at any point, ε_{cf}^{pl} and ε_{cf}^{in} are the plastic and inelastic strains, respectively. The term ε_{cf} represents the compressive strain after the elastic region of the compressive stress–strain diagram, whereas f_{c0} is the maximum elastic stress, which was assumed to be $0.5\,f_{cf}^{'}$, E_o is the elastic modulus of concrete, and the constant b_c was selected by Birtel and Mark [32] to be 0.7.

The tensile damage parameter is defined in terms of the ratio of post-cracking stress $f_{t(post-cracking)}$ to the ultimate tensile stress $f_t^{'}$, as in Eq. (2) [33]:

$$d_t = 1 - \frac{f_{t(post-cracking)}}{f_t^{'}} \tag{2}$$

Several studies recommended the Poisson's ratio of concrete to be in

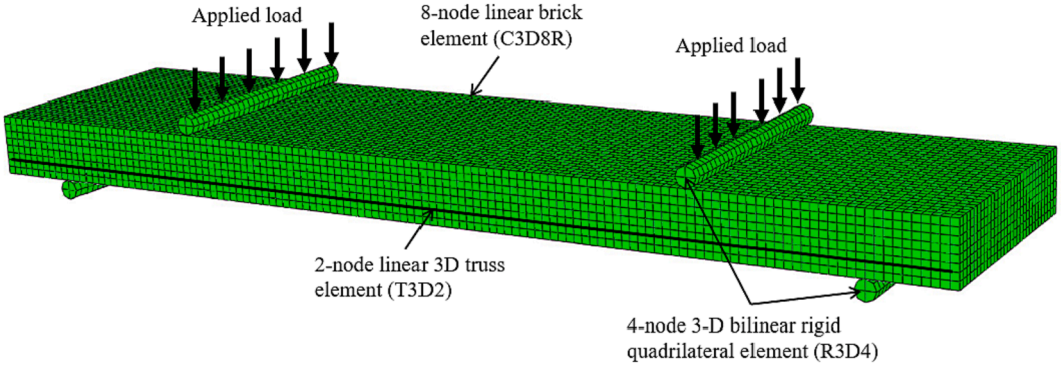

Fig. 1. Finite element modeling of BFRC-BFRP one-way slab.

the range from 0.14 to 0.26 [34], therefore the Poisson's ratio was selected to be 0.2.

The geometric FE modeling of the concrete slabs is shown in Fig. 1. A discrete rigid element, 4-node 3-D bilinear rigid quadrilateral element (R3D4), was employed to model the loading points and supports. Concrete was modeled using an 8-node linear brick element (C3D8R) with reduced integration. The BFRP bars were defined as a 2-node linear 3D truss element (T3D2) with an elastic behavior up to the ultimate tensile strength. The interface between FRP bars and concrete was modeled using an embedded element constraint. According to the Abaqus Analysis User's Guide [35], the embedded element can be used to model rebar reinforcement embedded in a three-dimensional solid (continuum) element called the host element. Therefore, several studies have applied the embedded element approach and achieved satisfactory results [34,36–39]. This option reflects the assumption of a fully bonding characteristic between the FRP bars and the surrounding concrete. When an embedded element option is used, Abaqus searches for the geometric relationships between the nodes of the embedded elements and the host elements. If Abaqus found that these nodes are lying within a host element, the translational degrees of freedom at these nodes are eliminated and the nodes become embedded nodes. Thus, the translational degrees of freedom of reinforcement truss nodes are constrained to the translational degrees of freedom of the surrounding concrete nodes. For the supports, an ENCASTRE boundary condition, as defined in ABAQUS, was imposed to restrict their movement in any direction. To select the proper FE mesh size for concrete, a mesh sensitivity analysis was carried out on different sizes of the 3D elements, namely 10, 20, 30, and 40 mm side lengths to ensure convergence and minimize the computational time. Accordingly, a mesh size of 20 mm was adopted as it was noticed to converge to a similar numerical value as that of the 10 mm mesh size with a lesser computational time. The discrete rigid and the truss elements used for point loads and BFRP bars, respectively, were assigned a similar mesh size so that the same nodes will be shared by different materials as recommended by [40,41].

2.1.1. The constitutive models

2.1.1.1. Concrete compressive stress–strain behavior. The non-linear compressive stress–strain behavior of BFRC was modeled by adopting Ayub et al. [42] model, where the analysis in this study was carried out based on concrete mixes containing up to 3% volume fraction of basalt macro fibers. The complete definition of this model is based on two proposed equations. The first equation (Eq. (3)) was utilized to predict the behavior for $0 < \varepsilon_{cf} \leq \varepsilon_{cf,lim}$ as shown in Fig. 2:

$$f_{cf} = \frac{n\beta f_{cf}^{'}\left(\varepsilon_c/\varepsilon_{of}\right)}{n\beta - 1 + \left(\varepsilon_c/\varepsilon_{of}\right)^{n\beta}} \tag{3}$$

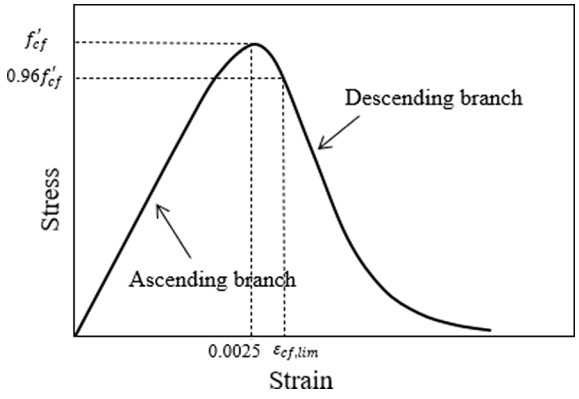

Fig. 2. Concrete compressive stress–strain model based on [42].

where ε_c is the strain at any point, $\varepsilon_{cf,lim}$ refers to the strain corresponding to the limiting stress of $0.96f_{cf}^{'}$ in the initial descending branch, while the strain ε_{of} corresponds to the peak stress $(f_{cf}^{'})$ and was chosen to be 0.0025 as suggested by Obaidat et al. [43]. In Eq. (3), n and β are material parameters, where n is related to the toughness of the stress–-strain curve and selected to be 3 based on Ayub et al. [42], while β is a shape factor that determines the initial ascending and descending curve of the stress–strain relationship, given by Hsu et al. [44] as:

$$\beta = \frac{1}{1 - \left(E_{cf}/E_o\right)} \qquad (for\ BFRC\ specimens) \tag{4a}$$

$$\beta = \left(\frac{f_{cf}^{'}}{65.23}\right)^{3} + 2.59 \qquad (for\ plain\ concrete\ specimens) \tag{4b}$$

The term E_{cf} is the secant elastic modulus and is calculated as $f_{cf}^{'}/\varepsilon_{of}$ and E_o is determined as illustrated below:

$$E_o = (10300 - 400V_f)\sqrt[3]{f_{cf}^{'}} \tag{5}$$

For $\varepsilon_{cf} > \varepsilon_{cf,lim}$, Eq. (6) was used to describe the stress–strain behavior in the final descending branch:

$$f_{cf} = f_{cf,lim} \times exp\left[\left(1 - n + 0.1V_f^2\right) \times \left\{\frac{\varepsilon_{cf}}{\varepsilon_{of}} - \frac{\varepsilon_{cf,lim}}{\varepsilon_{of}}\right\}^{1-0.1V_f}\right] \tag{6}$$

The toughness of the curve beyond the point $(\varepsilon_{cf,lim},\ 0.96f_{cf}^{'})$ was measured by the parameter: $1 - n + 0.1V_f^2$, whereas the parameter: $1 - 0.1V_f$ was used to determine the shape of the curve.

2.1.1.2. Concrete tensile stress–strain behavior. The literature lacks a study on the tensile stress–strain behavior of BFRC. However, a recent stress–strain preditive model for concrete containing polyvinyl alcohol (PVA) fibers was proposed by Khan and Ayub [45], as shown in Fig. 3. This model in combination with the model of Wang and Hsu [46] was adopted in this study to represent the complete response of BFRC under tension. As shown in Fig. 3a, the ascending behavior in the pre-cracking branch is not entirely linear but attains strain-hardening before the peak stress to consider the effect of fiber debonding. The pre-cracking part of the tensile stress–strain curve was obtained based on Eq. (7):

$$f_t = \frac{\omega f_t^{'}\left(\varepsilon_t/\varepsilon_{cr}\right)}{\omega - 1 + \left(\varepsilon_t/\varepsilon_{cr}\right)^{\omega}} \tag{7}$$

where f_t and ε_t are the tensile stress and strain at any point, ε_{cr} is the cracking strain, and $f_t^{'}$ is the peak tensile stress given by Eq. (8) [47–49] for plain concrete, while ω is a material parameter obtained according to Eq. (9).

$$f_t^{'} = 0.33\sqrt{f_{cf}^{'}} \tag{8}$$

$$\omega = 1.5E_o\varepsilon_{cr} \tag{9}$$

The contribution of BMF to the tensile strength of BFRC (σ_{cu}) was estimated by Adhikari [50] as in Eq. (10).

$$\sigma_{cu} = N_{fib}F_p \tag{10a}$$

$$N_{fib} = \frac{V_f}{\frac{\pi}{4}d_f^2}\alpha\eta_l \tag{10b}$$

$$F_p = \tau\pi d_f\frac{l_f}{4} \tag{10c}$$

$$\tau = \frac{\sigma_f d_f}{4l_f} \tag{10d}$$

where N_{fib} represents the effective number of randomly oriented fibers in a unit area, F_p is the pull-out force for an individual BMF strength,

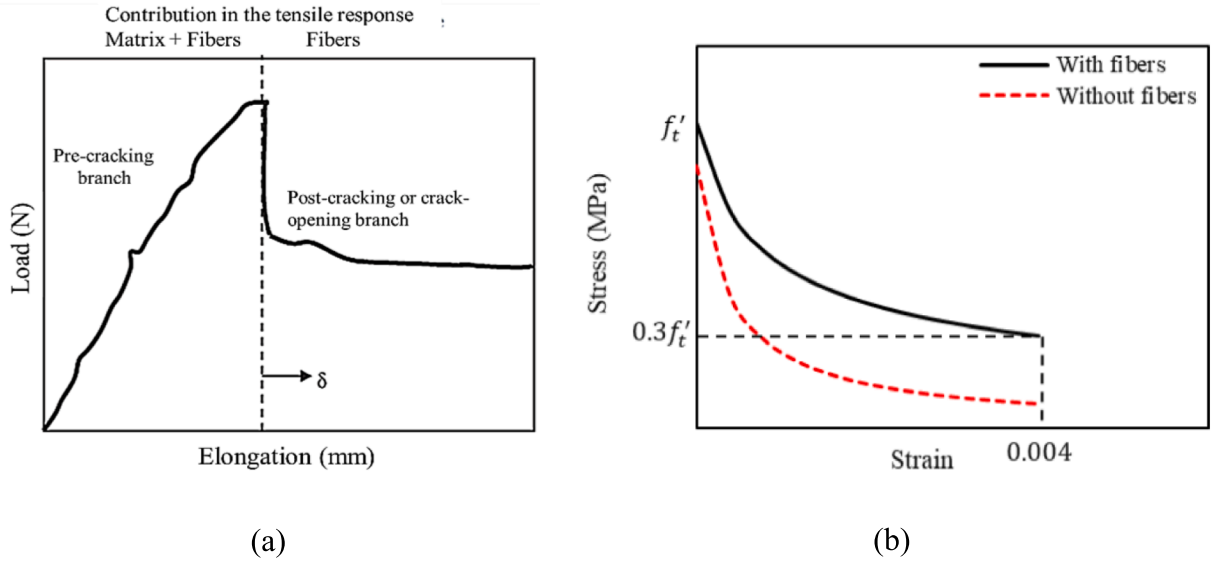

Fig. 3. Tensile stress–strain behavior of concrete: (a) stress–strain description according to the model of Khan and Ayub [45]; (b) the implemented stress–-strain model.

α and η_l account for the random orientation of fibers and the variability of their embedment length crossing any cracked plane and were taken as 3/8 [51] and 0.5 [52], respectively. The τ, σ_f, l_f, and d_f are the shear-bond strength, the tensile strength, the total length, and the diameter of BMF, respectively. According to the manufacturer's datasheet [53], σ_f= 1000 MPa, d_f = 0.66 mm, and l_f = 43 mm (See Fig. 4).

Fig. 4. Basalt macro fibers (BMF).

The onset of cracks in plain concrete induces a rapid dissipation of stress resulting from converting energy stored in concrete into fracture energy [54], whereas due to the bonding effect of reinforcing bars between the existed cracks, the softening part of the stress–strain curve is augmented by tension stiffening which consequently causes the stress to be gradually dissipated. This behavior would even be clearer in FRC specimens due to the presence of fibers that are bridging the formed cracks. Therefore, the drop of load in the post-cracking stage was modeled using Wang and Hsu [46] model, as given in Eq. (11) and shown in Fig. 3:

$$\sigma_t = \sigma_{t0}\left(\frac{\varepsilon_{cr}}{\varepsilon_t}\right)^{0.5}, \varepsilon_t > \varepsilon_{cr} \tag{11}$$

where the cracking strain ε_{cr} was calculated by dividing the maximum concrete tensile strength ($f_t^{'}+\sigma_{cu}$ (if any)) by the concrete elastic modulus E_o. However, it is worth mentioning here that when Khan and Ayub [45] conducted a single fiber pull-out test to observe the post-cracking response of the FRC specimen, their test results showed that upon cracking, there was a partial drop in the peak load. This was associated with strain elongation up to failure. Hence, for this study, 30% of $f_t^{'}$ was considered for BFRC specimens after concrete cracking as a residual tensile strength with a strain capacity of 0.004, as shown in Fig. 3b.

2.2. The simulated experimental program

The simulated experimental program involves four large-scale one-way concrete slabs tested by El-Sayed et al. [12] and Al-Hamrani and Alnahhal [25]. Table 1 summarizes the details of the specimens along with the mechanical characteristics of the FRP reinforcing bars. All

Table 1
Details of experimental tests from the literature.

	Bar type	$f_{cf}^{'}$(MPa)	b(mm)	d(mm)	a(mm)	No. and sizes of bars	f_{fu}(MPa)	E_{fu}(GPa)	V_f(%)
S-G2 [12]	GFRP	40	1000	158.9	1000	7ϕ22 mm	540	40	0
S-C1 [12]	CFRP	40	1000	165.25	1000	9ϕ10 mm	1536	114	0
SCB-ρ_1-0% [25]	BFRP	55.12	600	119	400	5ϕ12 mm	1177	49.48	0
SCB-ρ_1-0.75% [25]	BFRP	55.33	600	119	400	5ϕ12 mm	1177	49.48	0.75

b = slab width; a = shear span length; f_u = Ultimate tensile strength of longitudinal bars; E_{fu} = Elastic modulus of longitudinal bars; V_f = volume fraction of BMF.

specimens were tested under four-point loading. El-Sayed et al. [12] have evaluated the shear strength of one-way concrete slabs reinforced with different types of FRP bars. For example, slabs S-G2 and S-C1 were both cast with plain concrete and longitudinally reinforced with GFRP and CFRP bars, respectively, as listed in Table 1. More recently, Al-Hamrani and Alnahhal [25] investigated the shear behavior of one-way plain and BFRC slabs longitudinally reinforced with BFRP bars. The simulated slabs, namely SCB-ρ_1-0% and SCB-ρ_1-0.75% were cast with plain concrete and concrete mixed with 0.75% volume fraction of BMF, respectively.

2.3. Validation results

The FE model successfully predicted the transition point from pre-cracking into post-cracking behavior. By referring to Table 2, it can be observed that the cracking load and its corresponding deflection were in good agreement with the experimental observations. Although the numerical models were noticed to slightly under-estimate the ultimate loading capacity of slabs S-C1 and S-G2 [12], the numerical load–deflection diagrams were noticed to follow the experimental curves accurately at the remaining loading stages, as illustrated in Fig. 5. The numerical models have shown satisfactory predictions of the maximum experimental shear capacities with an average ratio of numerical shear capacity to experimental shear capacity (V_{num}/V_{exp}) of 0.95 ± 0.10 and a coefficient of variation (COV) of 10.30%. The models have also shown satisfactory predictions of the failure point and the maximum experimental displacements with an average ratio of maximum numerical displacement to maximum experimental displacement ($\Delta_{num}/\Delta_{exp}$) of 1.08 ± 0.15 and COV of 13.5%. It is worth noting that the failure point in all simulations was identified as the point at which the load dropped significantly. Fig. 6 shows that the developed numerical models have captured almost a similar crack response to that in the actual tests. Hence, it can be concluded that the developed model can be implemented to investigate the performance of one-way BFRC-

Table 2
Comparison between the numerical and experimental loads and displacements.

At cracking load, P_{cr} (kN)						
	$P_{cr,exp}$	$P_{cr,num}$	$P_{cr,num}/P_{cr,exp}$	Δ_{exp}(mm)	Δ_{num} (mm)	$\Delta_{num}/\Delta_{exp}$
S-G2 [12]	44.0	41.2	0.94	2.25	1.86	0.83
S-C1 [12]	45.0	41.6	0.92	2.60	2.14	0.82
SCB-ρ_1-0% [25]	22.5	19.3	0.86	2.50	2.04	0.82
SCB-ρ_1-0.75% [25]	25.5	23.5	0.92	2.28	2.58	1.13
At ultimate shear, V (kN)						
	V_{exp}	V_{num}	V_{num}/V_{exp}	Δ_{exp}(mm)	Δ_{num} (mm)	$\Delta_{num}/\Delta_{exp}$
S-G2 [12]	142	125.4	0.88	44.9	45.1	1.00
S-C1 [12]	140	120.4	0.86	57.6	55	0.95
SCB-ρ_1-0%[25]	69.8	70.4	1.01	37.1	47.4	1.28
SCB-ρ_1-0.75%[25]	81.5	86	1.06	43.5	47.3	1.09
Mean			0.95			1.08
SD			0.10			0.15
COV (%)			10.3			13.5

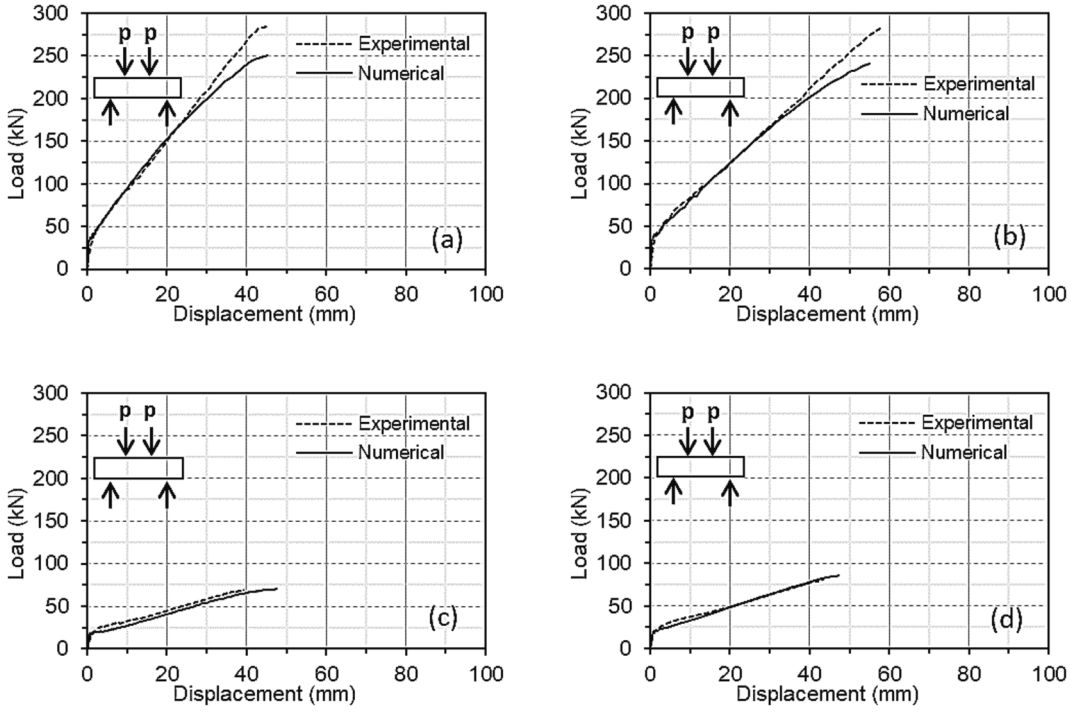

Fig. 5. Experimental versus numerical load–displacement response for (a) Specimen S-G1 from [12], (b) Specimen S-C1 from [12], (c) Specimen SCB-ρ_1-0% from [25] , and (d) Specimen SCB-ρ_1-0.75% from [25].

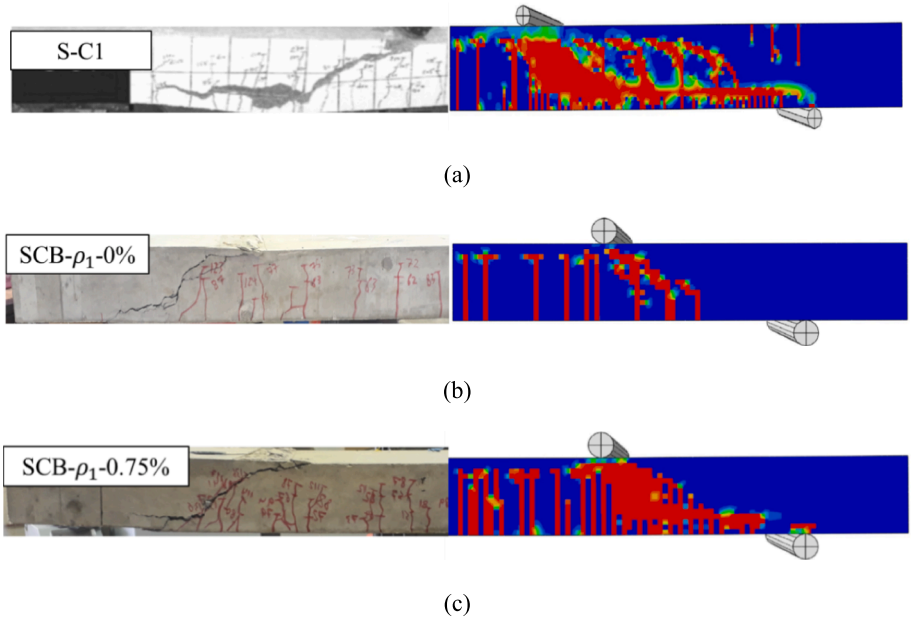

Fig. 6. The cracks patterns (experimental versus numerical) for: (a) Specimen S-C1 from [12], (b) Specimen SCB-ρ_1-0% from [25], and (c) Specimen SCB-ρ_1-0.75% from [25].

BFRP slabs.

3. Sensitivity analysis

Determining the shear behavior is technically challenging, and researchers have not addressed this subject for FRP-RC one-way slabs in much detail. Hence, to enrich this research area, a sensitivity analysis was implemented in this section to generate parameter combinations that were not included in the original FEM-validated experimental work. Then, the generated combinations were modelled using the virtual experimentation using the FEM to flexibly run these experiments and develop a mathematical expression for the shear strength of one-way BFRC-BFRP slabs.

3.1. Key parameters and fractional factorial design of experiment

Five main parameters influencing the shear capacity of one-way BFRC-BFRP slabs have been selected for sensitivity analysis, as listed in Table 3. These parameters are: 1) the longitudinal reinforcement ratio (ρ_{frpl}); 2) the concrete compressive strength ($f_{cf}^{'}$); 3) the shear span-to-depth (a/d) ratio; 4) the volume fraction of BMF (V_f); and 5) the effective depth (d) of slab. To systematically investigate the significance of the five input parameters and their two-way interactions on the response variable, which is the ultimate shear capacity, a widely used method, namely the three-level (3^k) fractional factorial DOE was utilized in this study [55,56], where k represents the number of parameters [55]. In multi-variable studies, factorial DOE is commonly used as the most efficient method to identify the significant factors and interactions that influence the response variable [55–57]

The levels of each parameter are selected based on a thorough literature review on FRP-RC slabs [9,12,15–19,58]. The width of all slabs was fixed to 1000 mm as this is a common unit strip width used in designing and analyzing one-way slabs. The distance from the center of the main reinforcement to the extreme tension layer was selected to be 30 mm. Moreover, the V_f of BMF was selected to be in the range from 0 to 2% as this range was common among several researchers [59–62], and using higher V_f values might impede the concrete workability.

A 3^k fractional factorial DOE of the five parameters resulted in 56 combinations of the parameters, which represent 56 BFRC-BFRP one-way slabs. The analysis of variance (ANOVA) [55] was then used to determine the significance of the effect of the input parameters and their possible interactions on the response variables at a significant level (α) of 5% using a two-way confidence interval of 95%. Thus, the significant level, which is a threshold that gives us a criterion to reject the null hypothesis (i.e., the effect is not significant), is set equal to 0.05. Accordingly, the effect of each parameter or interaction is said to be statistically significant when the corresponding P-value, which is the smallest level of significance at which the data are significant, is less than or equal to 0.05, whereas effects having P-values greater than 0.05 are not significant [55].

3.2. Identifying the significance of key parameters and interactions

Table 4 presents the results of the ANOVA analysis for the response variable. In addition, the normal probability plot in Fig. 7 shows the standardized effects of the design parameters relative to a distribution fit line that follows a normal distribution with zero mean value. The fit line indicates where the parameters would be if their effects were zero. The effect of a parameter is considered to be negligible if it is on or near the fit line, whereas its significance increases as the distance from the fit line

Table 3
The main parameters and their levels considered in the 3^k fractional factorial DOE.

The investigated parameters		Label	Lower level (−)	Average level (0)	Upper level (+)	Unit
Effective depth	d	A	100	160	220	mm
Shear span-to-depth ratio	a/d	B	3	4.25	6	–
Concrete compressive strength	$f_{cf}^{'}$	C	30	45	60	MPa
Volume fraction of fiber	V_f	D	0	1	2	%
Longitudinal BFRP reinforcement ratio	ρ_{frpl}	E	0.39	2.09	3.78	%

Table 4
The P-values of main parameters and their two-way interaction.

Label	Paraameters	P-value
		Shear capacity
A	d	**< 0.0001**
B	a/d	**< 0.0001**
C	f'_{cf}	**< 0.0001**
D	V_f	**< 0.0001**
E	ρ_{frpl}	**< 0.0001**
Two-way interactions		
AB	$d \times a/d$	**0.0077**
AC	$d \times f'_{cf}$	**0.0201**
AD	$d \times V_f$	**0.0463**
AE	$d \times \rho_{frpl}$	**0.0026**
BC	$a/d \times f'_{cf}$	0.1847
BD	$a/d \times V_f$	0.861
BE	$a/d \times \rho_{frpl}$	0.2748
CD	$f'_{cf} \times V_f$	0.3945
CE	$f'_{cf} \times \rho_{frpl}$	0.152
DE	$V_f \times \rho_{frpl}$	0.4382

increases. From the normal probability plots, it can also be distinguished whether a certain parameter has a positive or a negative effect on the response variable. For instance, the parameters that appear to be to the right of the fit line would have a positive effect, which indicates a direct relationship that increases or decreases the response as its value increases or decreases, respectively. In contrast, the parameters that appear to be to the left of the straight line would have a negative effect that decreases the response as its value increases. Moreover, the percentage contribution of the main parameters and their interaction to the shear capacity is shown in Fig. 8.

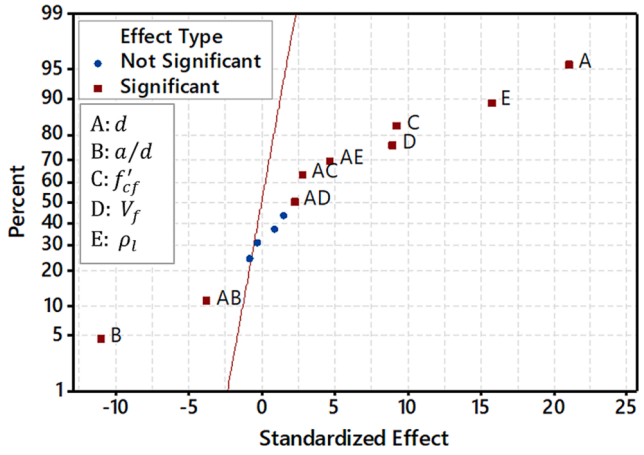

Fig. 7. Normal probability plots of the standardized effects.

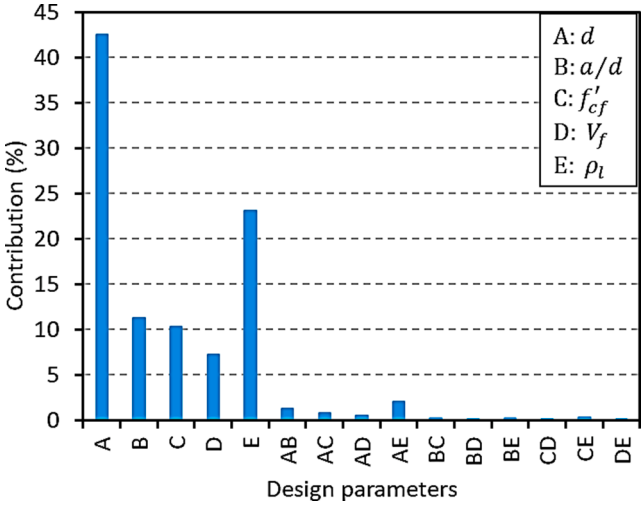

Fig. 8. Percent contribution of each design parameter on the shear capacity.

All main parameters showed a significant effect on the shear capacity at a significance level of 0.05, as listed in Table 4. In addition, the interaction of effective depth with shear span-to-depth ratio, concrete compressive strength, volume fraction of BMF, and longitudinal reinforcement ratio showed significant effects on the shear capacity of the BFRC-BFRP one-way slab, as presented in Table 4. In addition, as observed in Fig. 7, the parameters d, ρ_{frpl}, f'_{cf}, and V_f showed positive significant effects, while a/d ratio showed a negative significant effect on the shear capacity. According to Fig. 8, the d, ρ_{frpl}, and f'_{cf} factors exhibited significantly higher contribution to the shear capacity than the rest of the parameters and interactions, where their percent contribution was estimated to be 42.5%, 23.07%, and 10.3%, respectively. Fig. 7 is clearly showing the correlation between the input factors and the response variables, where the shear capacity is increasing as the d, ρ_{frpl}, and f'_{cf} factors are increasing, respectively. This finding is consistent with the shear design equations available in the current codes and design guidelines for FRP-RC sections, namely the ACI 440.1R-15 [63], CSA-S806-12 [64], JSCE-1997 [65], and ISIS-2007 [66], where they consider the d, ρ_l, and f'_{cf} factors as the main factors influencing the shear capacity. Previous test results also confirmed the obtained results. Abdul-Salam et al. [15], as an example, reported a 25% increase in the ultimate shear capacity of GFRP-RC one-way sabs when the ρ_l was increased from 2.62% to 3.78%. The improved shear strength at higher ρ_l values is referred to the boosted dowel capacity, which reduces the width and the penetration depth of the shear crack, thus, improving the shear resistance resulting from the aggregate interlock and the higher area of uncracked concrete in the compression zone [27]. Furthermore, El-Sayed et al. [26] reported that the increase in compressive strength from 43.6 MPa to 63 MPa has increased the shear capacity by 10.7%, 12.3%, and 4.4% for RC beams reinforced with steel, GFRP, and CFRP bars, respectively. Such observation was expected because the concrete peak tensile strength (f_t), which depends mainly on the f'_{cf}, is a major parameter affecting the concrete shear strength (V_c) [26]. Another important finding from Fig. 7 is that the a/d ratio was found to show a negative contribution on the shear capacity, which was estimated to be 11.27% as shown in Fig. 8. This was confirmed from several researchers [28,67–69], where they have shown that using higher values of a/d causes a reduction in the ultimate shear capacity. Additionally, it was found in this study that the V_f had a contribution of 7.26%. A comparison of this finding with those of other previous studies [59,70,71] confirmed that the addition of BMF enhances the shear capacity due to the bridging mechanism of BMF along the cracked surface. However, their tested specimens demonstrated a decrease in the rate of increase in shear capacity in specimens with a higher reinforcement ratio, indicating that the reinforcement ratio, rather than the fibers, was controlling the shear capacities of the tested beams.

Moreover, the ANOVA analysis identified the significant interaction effect among parameters, namely $d \times \rho_{frpl}$, $d \times f'_{cf}$, $d \times V_f$, and $d \times a/d$ with corresponding contributions of 2.04%, 1.27%, 0.81%, and 0.53%. The $d \times f'_{cf}$, $d \times \rho_{frpl}$, and $d \times V_f$ interaction showed positive significant effects, as shown in Fig. 7. This is because, at a larger effective depth and flexural reinforcement ratio, a larger compression zone is necessary to achieve the equilibrium requirement in a cross-section. As a result, this will enhance the contribution of the uncracked compression zone of a certain compressive strength to shear capacity [72]. Moreover, increasing the volume fraction of BMF in a certain effective depth will result in a greater number of BMF crossing and resisting the widening of the diagonal shear cracks, thus, improving the aggregate interlock

between the cracked surfaces and resulting in higher shear capacity [59]. On the other hand, the $d \times a/d$ interaction showed negative significant effect, which indicates lesser influence of d at longer a/d ratios. This could be connected to the tendency of the slab to fail under flexure than failing under shear due to higher flexural stresses at longer a/d ratios[59].

4. The proposed shear design equation

The genetic algorithm (GA) has emerged as a powerful optimization strategy, which searches for the optimal solution for a certain problem by mimicking Darwin's principle of natural selection and the survival of the fittest [73]. The GA approach begins with a random group of coded individuals (solutions), each of which is known as a chromosome and is filled with genes. In each generation, the fittest individuals mate to yield better individuals for the successor generation through a set of mathematical operations deduced from biological processes, namely selection, crossover, and mutation [74]. By repeating this genetic cycle, the quality of the offspring solutions gradually improves until reaching the optimal solution, where no further improvement can be observed for newer generations.

In the current study, an equation that can predict the shear strength of plain and BFRC-BFRP one-way slabs was developed via the GA technique. For the equation development, the database results of the same 56 combinations resulting from the (3^k) fractional factorial DOE were used to fit the objective function shown in Eq. (12), which defines the relationship between the dependent and independent variables. It can be noticed that the presented model in Eq. (12) is comprised of two parts to indicate the independent contribution to shear strength resulting from concrete (v_c) and fibers (v_{fib}).

$$v_{c,f} = v_c + v_{fib} \tag{12a}$$

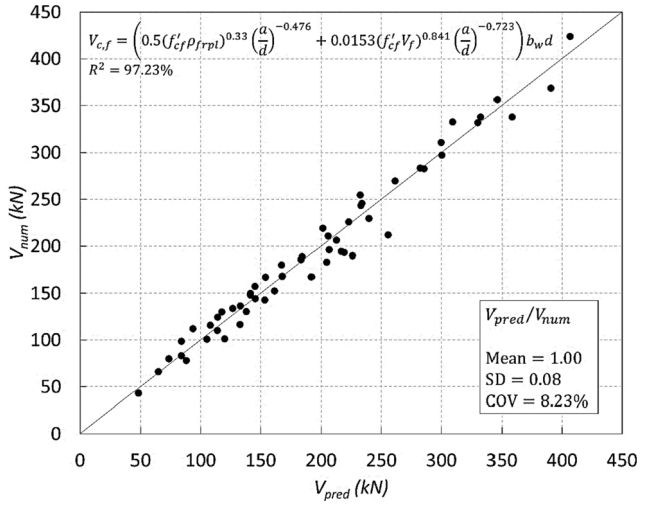

Fig. 9. Predicted Vs numerical shear capacities of the 56 modelled one-way BFRC-BFRP slabs.

$$v_{c,f} = c_1\left(f'_{cf}\rho_{frpl}\right)^{c_2}\left(\frac{a}{d}\right)^{c_3} + c_4\left(f'_{cf}V_f\right)^{c_5}\left(\frac{a}{d}\right)^{c_6} \tag{12b}$$

where ρ_{frpl} and V_f are in percentages, and c_1, c_2, c_3, c_4, c_5, and c_6 are the unknown terms to be determined based on the results of GA analysis. After running the GA analysis, the developed shear equation is given below:

$$V_{c,f} = \left(0.5\left(f'_{cf}\rho_{frpl}\right)^{0.33}\left(\frac{a}{d}\right)^{-0.476} + 0.0153\left(f'_{cf}V_f\right)^{0.841}\left(\frac{a}{d}\right)^{-0.723}\right)b_w d \tag{13}$$

By comparing the numerically obtained results of the 56 combinations with those predicted by Eq. 13, it can be seen according to Fig. 9 that Eq. 13 has well predicted the 56 numerical shear capacities with an average predicted to numerical shear capacity (V_{pre}/V_{num}) ratio of 1.00 ± 0.08, a low COV of 8.23%, and R^2 of 97.23% which is close to 100%.

4.1. Experimental verification and comparison

For the validation of the proposed model, an experimental database of 49 one-way slabs that failed in shear was collected [12,15,16,67,75,76]. The main variables of the collected database with their ranges are listed in Table 5. Two types of FRP bars were considered

Table 6
Design codes and guidelines.

Design code/ guideline	Equations	
ACI 440.1R-15 [63]	$V_c = \frac{2}{5}\sqrt{f'c}\,b_w kd$ $k = \sqrt{2\rho n + (\rho n)^2} - \rho n$ b_w = slab width n = ratio of modulus of elasticity of FRP bars to modulus of elasticity of concrete	(14)
CSA-S806-12 [64]	$V_c = 0.05\lambda k_m k_r (f'c)^{\frac{1}{3}} b_w d_v$, *for* $d \le 300$ *mm* where $0.11\sqrt{f'c}\,b_w d_v \le V_c \le 0.22\sqrt{f'c}\,b_w d_v$ d_v is the maximum of $0.9d$ or $0.72h$ h is the overall thickness of a member $k_m = \sqrt{\frac{V_f d}{M_f}} \le 1.0$, where $\left(\frac{V_f d}{M_f}\right)$ is equivalent to $\left(\frac{d}{a}\right)$ $k_r = 1 + (E_f\rho)^{\frac{1}{3}}$	(15)
JSCE-97 [65]	$V_c = \beta_d\beta_p\beta_n f_{vcd} b_w d/\gamma_b$ $\beta_d = \left(\frac{1000}{d}\right)^{\frac{1}{4}} \le 1.5$ $\beta_p = \left(\frac{1000\rho_{frpl}E_f}{E_s}\right)^{\frac{1}{4}} \le 1.5$ $\beta_n = 1$ if no axial force applied $f_{vcd} = 0.2\sqrt[3]{f'c}$ provided that $f_{vcd} \le 0.72\frac{N}{mm^2}$ $\gamma_b = 1.3$	(16)
ISIS 2007 [66]	$V_c = 0.2\lambda\sqrt{f'c}\,b_w d\sqrt{\frac{E_f}{E_s}}$ E_s = Elastic modulus for steel E_f = Elastic modulus for FRP	(17)

Table 5
Details of the experimental database.

Investigator	Number of specimens	FRP type	b(mm)	d (mm)	a/d	f'_c(MPa)	ρ_{frpl}(%)	V_f(%)	V_{exp}(kN)
El-Sayed et al.[12]	5	GFRP	1000	152.6–162.1	6.17–6.55	40	0.86–2.63	0	113–168
Abdul-salam et al.[15]	10	GFRP	1000	134.9–143	5.95–6.21	42.9–82.6	0.8–3.78	0	94–213
Chang and Seo [16]	6	GFRP	1200	173.5	5.8	33	0.73–1.22	0	95–158.5
Issa et al. [67]	6	BFRP	300	165–170	5.65–7	35.9	0.8–4.12	0	29.3–51.5
Deitz et al. [75]	3	GFRP	305	158	4.5–5.8	26.8–29.2	0.73	0	26.8–29.2
Kilpatrick et al.[76]	12	GFRP	420	78–83	3.61–6.41	61–93	0.61–2.61	0	20–55.6
Al-Hamrani and Alnahhal [25]	7	BFRP	600	119	3.36	55	0.79–1.28	0–0.75	69.8–95.7

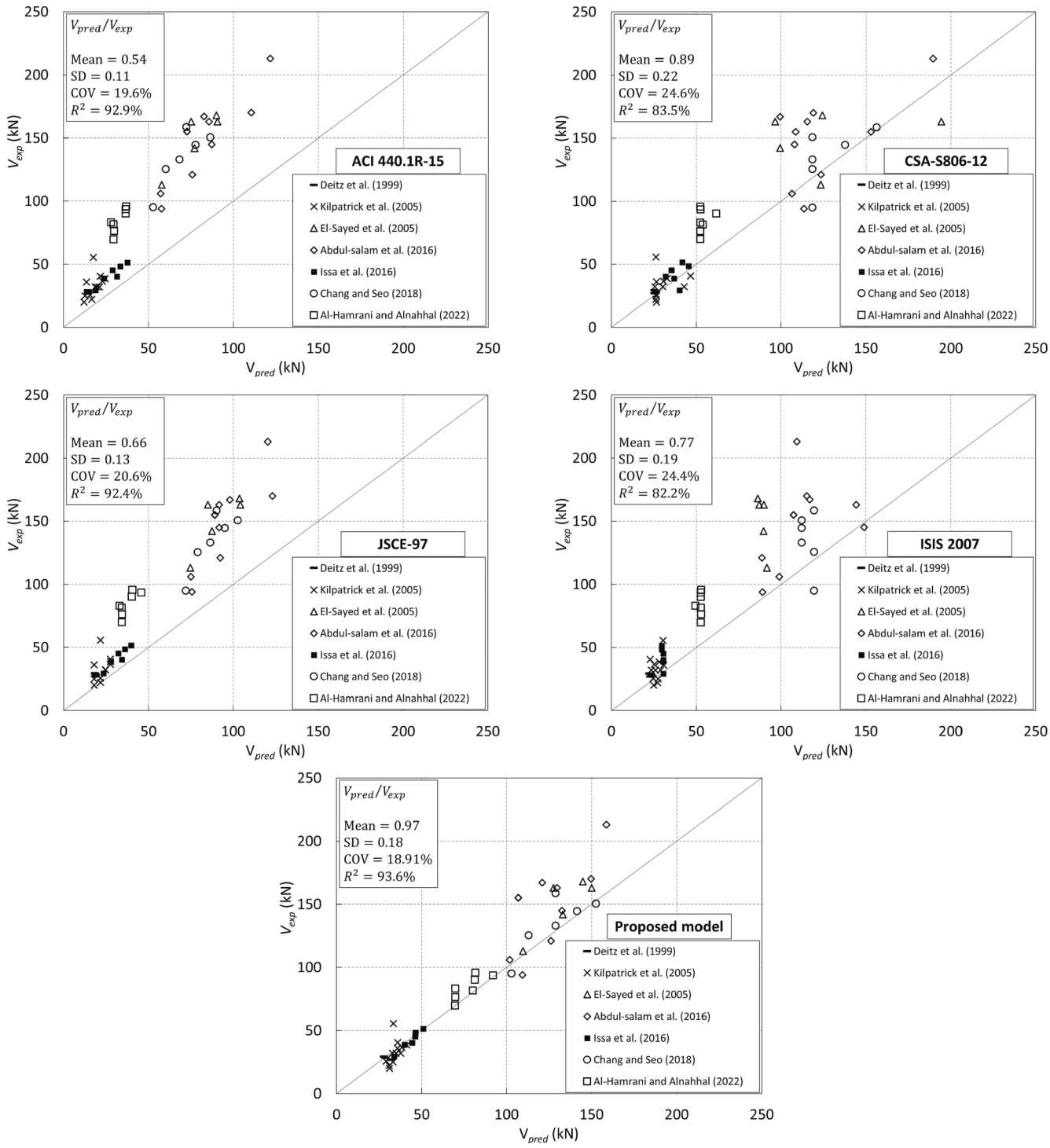

Fig. 10. Experimental Vs predicted shear capacities for the experimental database collected from the literature [12,15,16,25,67,75,76].

in this database, which are GFRP and BFRP bars due to their approximately similar mechanical characteristics. As can be observed from Table 5, most of the collected slabs were cast with plain concrete, whereas slabs with fibers were only found in [25].

Therefore, the prediction accuracy of the proposed model was compared with the available design codes and guidelines for plain concrete sections listed in Table 6, namely ACI 440.1R-15 [63], CSA-S806-12 [64], JSCE-97 [65], and ISIS 2007 [66]. By referring to Fig. 10, most of the ACI 440.1R-15 [63] predictions were over-conservative with a mean of the predicted to experimental shear capacity (V_{pred}/V_{exp}) ratio of 0.54 ± 0.11 and a COV of 19.6%. Likewise, the JSCE-97 [65] and ISIS 2007 [66] were also conservative, but to a lesser extent with mean V_{pred}/V_{exp} of 0.66 ± 0.13 and 0.77 ± 0.19, and COV of 20.6% and 24.4%, respectively. In contrast, CSA-S806-12 [64] demonstrated improved prediction accuracy with mean V_{pred}/V_{exp} of 0.89 ± 0.22 and COV of 24.6%. For the proposed model, most of the predicted values were found to be close to or exactly on the 45-degree line as demonstrated in Fig. 10. In addition, most of the slabs were conservatively predicted, however, the conservative degree of prediction was increasing for slabs experienced higher shear capacities, which was also noticed for the remaining models. Overall, Fig. 10 demonstrates that the proposed model has shown the best prediction accuracy in

predicting the experimental results with a mean V_{pred}/V_{exp} of 0.97 ± 0.18, a COV of 17.91%, and R^2 of 93.6%.

5. Conclusions

In this study, a 3D finite element modeling framework for the shear behavior of one-way BFRC slabs reinforced longitudinally with BFRP bars was presented and validated. Following validation, a sensitivity analysis was conducted on five key design parameters with their two-way interactions using a three-level fractional factorial design of experiment resulting in 56 combinations of the parameters. The significance of each parameter was then determined by employing the statistical test ANOVA with a two-sided confidence level of 95%. Finally, a mathematical expression that can predict the shear capacity of one-way BFRC-BFRP slabs was developed using a genetic algorithm. The following conclusions can be drawn from this study:

1- The highest positive contribution to the shear capacity was due to the effective depth, the longitudinal reinforcement ratio, and the compressive strength with percent contributions of 42.58%, 24.58%, and 10.30%, respectively. This finding was found to agree with those of the current codes and design guidelines for FRP-RC, namely the ACI 440.1R-15 [63], CSA-S806-12 [64], JSCE-1997 [65], and ISIS-2007 [66] as their shear design equations are considering these factors to have a primary effect on the shear capacity. In contrast, the statistical results showed a negative significant effect of the shear span-to-depth ratio with a contribution of 11.27%, which has been considered by the CSA-S806-12 [64] code.
2- The addition of BMF was also determined to be statistically significant with a percentage contribution of 7.26%. This could reflect the enhanced shear capacity of BFRC specimens as a result of the BMF crossing the diagonal shear crack, thus strengthening the cracked surface as reported in the literature.
3- Several two-way interactions were found to be statistically significant such as $d \times \rho_{frpl}$, $d \times f_{cf}^{'}$, and $d \times V_f$ with positive contributions of 2.04%, 1.27%, and 0.81%, respectively, while the interaction of $d \times a/d$ was determined to be statistically significant with a negative contribution of 0.53%.
4- The proposed model has shown the best prediction capability compared to the available design codes/guidelines with a mean V_{pred}/V_{exp} of 0.97 ± 0.18 and a COV of 17.91%. On the other hand, the ACI 440.1R-15 [63], JSCE-97 [65], and ISIS 2007 [66] have shown highly conservative predictions with mean V_{pred}/V_{exp} of 0.54 ± 0.11, 0.66 ± 0.13, and 0.77 ± 0.19, and COV of 19.6%, 20.6%, and 24.4%, respectively, whereas the CSA-S806-12 [64] has shown less conservative predictions with a mean V_{pred}/V_{exp} of 0.89 ± 0.22 and a COV of 24.6%.

CRediT authorship contribution statement

Abathar Al-Hamrani: Investigation, Formal analysis, Data curation, Software, Visualization, Conceptualization, Methodology, Validation, Writing – original draft, Writing – review & editing. **Tadesse G. Wakjira:** Investigation, Formal analysis, Data curation, Software, Visualization, Conceptualization, Methodology, Validation, Writing – original draft. **Wael Alnahhal:** Conceptualization, Methodology, Validation, Writing – review & editing, Resources, Funding acquisition, Supervision, Project administration. **Usama Ebead:** Writing – review & editing, Supervision, Project administration.

Declaration of Competing Interest

The authors declare that they have no known competing financial interests or personal relationships that could have appeared to influence the work reported in this paper.

Data availability

The raw/processed data required to reproduce these findings cannot be shared at this time as the data also forms part of an ongoing study.

Acknowledgement

The authors show their gratitude to Qatar Foundation for their financial support through the GSRA grant no. **GSRA6-1-0301-19005**, the UREP award no. **UREP21-089-2-039**, and the NPRP grant no. **NPRP 13S-0209-200311** from the Qatar National Research Fund (QNRF, a member of Qatar Foundation). O**pen access funding** was provided by the QatarNational Library (**QNL**).

***Data** Availability*

Data availability The raw/processed data required to reproduce these findings cannot be shared at this time as the data also forms part of an ongoing study.

References

[1] Balaguru PN, Nanni A, Giancaspro J. FRP composites for reinforced and prestressed concrete structures : a guide to fundamentals and design for repair and retrofit. 1st ed. Taylor & Francis; 2009.
[2] GangaRao HV., Taly N, Vijay P V. Reinforced Concrete Design with FRP Composite. 1st ed. 2006.
[3] Le TD, Pham TM, Hao H, Yuan C. Performance of precast segmental concrete beams posttensioned with carbon fi ber-reinforced polymer (CFRP) tendons. Compos Struct 2019;208:56–69. https://doi.org/10.1016/j.compstruct.2018.10.015.
[4] Maranan GB, Manalo AC, Karunasena W, Benmokrane B. Pullout behaviour of GFRP bars with anchor head in geopolymer concrete. Compos Struct 2015;132:1113–21. https://doi.org/10.1016/j.compstruct.2015.07.021.
[5] Monaldo E, Nerilli F, Vairo G. Basalt-based fiber-reinforced materials and structural applications in civil engineering. Compos Struct 2019;214:246–63. https://doi.org/10.1016/j.compstruct.2019.02.002.
[6] Abushanab A, Alnahhal W. Numerical parametric investigation on the moment redistribution of basalt FRC continuous beams with basalt FRP bars. Compos Struct 2021;277:114618. https://doi.org/10.1016/J.COMPSTRUCT.2021.114618.
[7] Abushanab A, Alnahhal W. Performance of Basalt Fiber Reinforced Continuous Beams with Basalt FRP Bars. IOP Conf. Ser. Mater. Sci. Eng., vol. 910, IOP Publishing Ltd; 2020, p. 012004. Doi: https://doi.org/10.1088/1757-899X/910/1/012004.
[8] Sim J, Park C, Moon DY. Characteristics of basalt fiber as a strengthening material for concrete structures. Compos Part B Eng 2005;36:504–12. https://doi.org/10.1016/j.compositesb.2005.02.002.
[9] Zheng Y, Zhou L, Taylor SE, Ma H. Serviceability of one-way high-volume fly ash-self-compacting concrete slabs reinforced with basalt FRP bars. Constr Build Mater 2019;217:108–27. https://doi.org/10.1016/j.conbuildmat.2019.05.044.
[10] Attia K, Alnahhal W, Elrefai A, Rihan Y. Flexural behavior of basalt fiber-reinforced concrete slab strips reinforced with BFRP and GFRP bars. Compos Struct 2019. https://doi.org/10.1016/j.compstruct.2018.12.016.
[11] Erfan AM, Elnaby RMA, Badr AA, El-sayed TA. Flexural behavior of HSC one way slabs reinforced with basalt FRP bars. Case Stud Constr Mater 2021;14. https://doi.org/10.1016/j.cscm.2021.e00513.
[12] El-sayed A, El-salakawy E, Benmokrane B. Shear Strength of One-Way Concrete Slabs Reinforced with Fiber-Reinforced Polymer Composite Bars. J Compos Constr 2005;9:147–57. https://doi.org/10.1061/(ASCE)1090-0268(2005)9.
[13] Wakjira TG, Al-Hamrani A, Ebead U, Alnahhal W. Shear capacity prediction of FRP-RC beams using single and ensenble ExPlainable Machine learning models. Compos Struct 2022;287. https://doi.org/10.1016/j.compstruct.2022.115381.
[14] Dhipanaravind SS, R.. Flexural Behaviour of Concrete Oneway Slabs Reinforced with Hybrid FRP Bars. Int J Appl Eng Res 2018;13:4807–15.
[15] Abdul-Salam B, Farghaly AS, Benmokrane B. Mechanisms of shear resistance of one-way concrete slabs reinforced with FRP bars. Constr Build Mater 2016;127:959–70. https://doi.org/10.1016/j.conbuildmat.2016.10.015.
[16] Chang K, Seo D. Behavior of one-way concrete slabs reinforced with GFRP bars. J Asian Archit Build Eng 2012;11:351–8. https://doi.org/10.3130/jaabe.11.351.
[17] Benmokrane B, El-salakawy E, Cherrak Z, Wiseman A. Fibre reinforced polymer composite bars for the structural concrete slabs of a Public Works and Government Services Canada parking garage 2005;748:732–48. Doi: https://doi.org/10.1139/L04-049.

[18] Michaluk CR, Rizkalla SH, Tadros G, Benmokrane B. Flexural behavior of one-way concrete slabs reinforced by fiber reinforced plastic reinforcements. ACI Struct J 1998;95:353–65. https://doi.org/10.14359/552.

[19] Abdulsalam B, Farghaly A, Benmokrane B. Evaluation of Shear Behavior for One-Way Concrete Slabs Reinforced with Carbon-FRP Bars. CSCE 2013 Gen. Conf. - Congrès général 2013 la SCGC, Montréal, Québec: 2013. Doi: https://doi.org/10.13140/RG.2.1.3831.7609.

[20] Sahoo DR, Maran K, Kumar A. Effect of steel and synthetic fibers on shear strength of RC beams without shear stirrups. Constr Build Mater 2015;83:150–8. https://doi.org/10.1016/j.conbuildmat.2015.03.010.

[21] High C, Seliem HM, El-Safty A, Rizkalla SH. Use of basalt fibers for concrete structures. Constr Build Mater 2015;96:37–46. https://doi.org/10.1016/j.conbuildmat.2015.07.138.

[22] Bajaj S. Effect of Corrossion on Physical and Mechanical Properties of Reinforced Concrete. University of Akron; 2012. Master thesis.

[23] Alnahhal W, Taha R, Alnuaimi N, Al-Hamrani A. Properties of fibre-reinforced concrete made with discarded materials. Mag Concr Res 2019. https://doi.org/10.1680/jmacr.17.00293.

[24] Krassowska J, Lapko A. The Influence of Steel and Basalt Fibers on the Shear and Flexural Capacity of Reinforced Concrete Beams. vol. 7. 2013.

[25] Al-Hamrani A, Alnahhal W. Shear Behaviour of One-way High Strength Plain and FRC Slabs Reinforced with Basalt FRP Bars. Compos Struct 2022;302. https://doi.org/10.1016/j.compstruct.2022.116234.

[26] El-Sayed AK, El-Salakawy EF, Benmokrane B. Shear capacity of high-strength concrete beams reinforced with FRP bars. ACI Struct J 2006;103:383–9. https://doi.org/10.14359/15316.

[27] El-Sayed AK, El-Salakawy EF, Benmokrane B. Shear Strength of FRP-Reinforced Concrete Beams without Transverse Reinforcement. ACI Struct J 2006;103:235–43. https://doi.org/10.14359/15181.

[28] Razaqpur AG, Isgor BO, Greenaway S, Selley A. Concrete Contribution to the Shear Resistance of Fiber Reinforced Polymer Reinforced Concrete Members. J Compos Constr 2004;8:452–60. https://doi.org/10.1061/(ASCE)1090-0268(2004)8:5(452).

[29] Cicekli U, Voyiadjis GZ, Al-rub RKA. A plasticity and anisotropic damage model for plain concrete. Int J Plast 2007;23:1874–900. https://doi.org/10.1016/j.ijplas.2007.03.006.

[30] Grassl P. Damage-plastic model for concrete failure. Int J Solids Struct 2006;43:7166–96. https://doi.org/10.1016/j.ijsolstr.2006.06.032.

[31] Lubliner J, Oliver J, Oliver S, Onate E. A plastic-damage model for concrete.pdf. Int J Solids Struct 1989;25:299–326.

[32] Birtel V, Mark P. Parameterised Finite Element Modelling of RC Beam Shear Failure. Ababqus User's Conf. 2006:95–108.

[33] Malm R. Predicting shear type crack initiation and growth in concrete with non-linear finite element method. Royal Institute of Technology (KTH); 2009.

[34] Bahroz G, Ramadhan A. Numerical modeling of size effect in shear strength of FRP-reinforced concrete beams. Structures 2019;20:237–54. https://doi.org/10.1016/j.istruc.2019.04.008.

[35] Abaqus Analysis User's Guide (Simulia-Abaqus 6.13) 2013.

[36] Kadhim MMA, Jawdhari AR, Altaee MJ, Adheem AH. Finite element modelling and parametric analysis of FRP strengthened RC beams under impact load. J Build Eng 2020:32. https://doi.org/10.1016/j.jobe.2020.101526.

[37] Tahzeeb R, Alam M, Muddassir SM. A comparative performance of columns: reinforced concrete, composite, and composite with partial C-FRP wrapping under contact blast. Mater Today Proc 2022;62:2191–202. https://doi.org/10.1016/j.matpr.2022.03.367.

[38] Alnajmi L, Abed F. Evaluation of FRP bars under compression and their performance in RC columns. Materials (Basel) 2020;13:1–19. https://doi.org/10.3390/ma13204541.

[39] Tran DT, Pham TM, Hao H, Chen W. Numerical study on bending response of precast segmental concrete beams externally prestressed with FRP tendons. Eng Struct 2021:241. https://doi.org/10.1016/j.engstruct.2021.112423.

[40] Metwally IM. Three-dimensional nonlinear finite element analysis of concrete deep beam reinforced with GFRP bars. HBRC J 2017;13:25–38. https://doi.org/10.1016/j.hbrcj.2015.02.006.

[41] Abed F, El Refai A, Abdalla S. Experimental and finite element investigation of the shear performance of BFRP-RC short beams. Structures 2019;20:689–701. https://doi.org/10.1016/j.istruc.2019.06.019.

[42] Ayub T, Asce SM, Shafiq N, Khan SU. Compressive Stress-Strain Behavior of HSFRC Reinforced with Basalt Fibers. J Mater Civ Eng 2016;28:1–11. https://doi.org/10.1061/(ASCE)MT.1943-5533.0001441.

[43] Obaidat YT, Heyden S, Dahlblom O. The effect of CFRP and CFRP / concrete interface models when modelling retrofitted RC beams with FEM. Compos Struct 2010;92:1391–8. https://doi.org/10.1016/j.compstruct.2009.11.008.

[44] Hsu L, Hsu C. Stress-strain behavior of steel-fiber high strength concrete under compression. ACI Struct J 1994;91:448–57.

[45] Khan SU, Ayub T. Modelling of the pre and post-cracking response of the PVA fibre reinforced concrete subjected to direct tension. Constr Build Mater 2016;120:540–57. https://doi.org/10.1016/j.conbuildmat.2016.05.130.

[46] Wang T, Hsu TTC. Nonlinear finite element analysis of concrete structures using new constitutive models. Comput Struct 2001;79:2781–91. https://doi.org/10.1016/S0045-7949(01)00157-2.

[47] Genikomsou AS, Polak MA. Finite element analysis of punching shear of concrete slabs using damaged plasticity model in ABAQUS. Eng Struct 2015;98:38–48. https://doi.org/10.1016/j.engstruct.2015.04.016.

[48] Hu H, Lin F, Jan Y. Nonlinear finite element analysis of reinforced concrete beams strengthened by fiber-reinforced plastics. Compos Struct 2004;63:271–81. https://doi.org/10.1016/S0263-8223(03)00174-0.

[49] Obaidat YT. Structural retrofitting of reinforced concrete beams using carbon fibre reinforced polymer. LUND University; 2010.

[50] Adhikari S. Mechanical and structural characterization of mini-bar reinforced concrete beams 2013.

[51] Foster SJ. On behavior of high-strength concrete columns: Cover spalling, steel fibers, and ductility. ACI Struct J 2001;98:583–9. https://doi.org/10.14359/10301.

[52] Aoude H. Structural Behaviour of Steel Fibre. Montreal, QC, Canada: Department of Civil Engineering and Applied Mechanics, McGill University; 2007. PhD thesis,.

[53] MST-BAR 2017.

[54] Nayal R, Rasheed HA. Tension Stiffening Model for Concrete Beams Reinforced with Steel and FRP Bars. J Mater Civ Eng 2006;18:831–41.

[55] Montgomery DC. Design and Analysis of Experiments. 8th ed. Hoboken, New Jersey, USA: John Wiley & Sons Inc; 2013.

[56] Wakjira TG, Nehdi ML, Ebead U. Fractional factorial design model for seismic performance of RC bridge piers retrofitted with steel-reinforced polymer composites. Eng Struct 2020:221. https://doi.org/10.1016/j.engstruct.2020.111100.

[57] Abdel Baky H, Ebead UA, Neale KW. Statistical analyses and parametric study for reinforced concrete beams strengthened in flexure with FRPs. Adv Struct Eng 2010;13:805–22. https://doi.org/10.1260/1369-4332.13.5.805.

[58] Abdulsalam B, Farghaly A, Benmokrane B. Evaluation of Shear Behavior for One-Way Concrete Slabs Reinforced with Carbon-FRP Bars Evaluation of Shear Behavior for One-Way Concrete Slabs Reinforced with Carbon-FRP Bars 2013. Doi: https://doi.org/10.13140/RG.2.1.3831.7609.

[59] AL-Hamrani A, Alnahhal W. Shear behavior of basalt FRC beams reinforced with basalt FRP bars and glass FRP stirrups: Experimental and analytical investigations. Eng Struct 2020;242:107. https://doi.org/10.29117/quarfe.2020.0081.

[60] Sarmah M, Roy B, Mozumder RA, Laskar AI. Effect of Chopped Basalt Fibers on the Cyclic Behavior of RCC Beam-Column Subassemblies. Arab J Sci Eng 2018;43:1865–74. https://doi.org/10.1007/s13369-017-2801-y.

[61] Jalasutram S, Sahoo DR, Matsagar V. Experimental investigation of the mechanical properties of basalt fiber-reinforced concrete. Struct Concr 2017;18:292–302. https://doi.org/10.1002/suco.201500216.

[62] Mohammadi Mohaghegh A, Silfwerbrand J, Årskog V. Shear behavior of high-performance basalt fiber concrete—Part I: Laboratory shear tests on beams with macro fibers and bars. Struct Concr 2018;19:246–54. https://doi.org/10.1002/suco.201700208.

[63] American Concrete Institute (ACI) Committee 440. Guide for the Design and Construction of Structural Concrete Reinforced with Fibre-Reinforced Polymer (FRP) Bars (ACI 440.1R-15). 2015. Doi: https://doi.org/10.1061/40753(171)158.

[64] CSA (Canadian Standards Association). Design and construction of building components with fiber reinforced polymers. (CSA-S806-12) 2012.

[65] JSCE (Japan Society of Civil Engineers). Recommendation for design and construction of concrete structures using continuous fiber reinforcing materials. Japan Soc. Civ. Eng., 1997, p. 1–58.

[66] ISIS (Intelligent Sensing for Innovative Structures). Reinforcing Concrete Structures with Fibre Reinforced Polymers. 2007.

[67] Issa MA, Ovitigala T, Ibrahim M. Shear Behavior of Basalt Fiber Reinforced Concrete Beams with and without Basalt FRP Stirrups. J Compos Constr 2016;20:04015083. https://doi.org/10.1061/(ASCE)CC.1943-5614.0000638.

[68] El Refai A, Abed F. Concrete contribution to shear strength of beams reinforced with basalt fiber-reinforced bars. J Compos Constr 2016;20:4015082. https://doi.org/10.1061/(ASCE)CC.1943-5614.0000648.

[69] Al-Hamrani A, Alnahhal W, Elahtem A. Shear behavior of green concrete beams reinforced with basalt FRP bars and stirrups. Compos Struct 2021;277:114619. https://doi.org/10.1016/J.COMPSTRUCT.2021.114619.

[70] Al-Hamrani A, Alnahhal W. The Influence of Reinforcement Ratio on the Shear Behaviour of Sand Coated Basalt FRP Bars Reinforced Beams. Lect. Notes Civ. Eng., vol. 198 LNCE, Springer International Publishing; 2022, p. 973–9. Doi: https://doi.org/10.1007/978-3-030-88166-5_85.

[71] El Refai A, Alnahhal W, Al-Hamrani A, Hamed S. Shear performance of basalt fiber-reinforced concrete beams reinforced with BFRP bars. Compos Struct 2022;288:115443. https://doi.org/10.1016/j.compstruct.2022.115443.

[72] Lantsoght EOL. How do steel fibers improve the shear capacity of reinforced concrete beams without stirrups? Compos Part B Eng 2019:175. https://doi.org/10.1016/j.compositesb.2019.107079.

[73] Holland JH. Adaptation in Natural and Artificial Systems. Adapt. Nat. Artif. Syst. 2019. https://doi.org/10.7551/mitpress/1090.001.0001.

[74] Xu B, Lin H, Wagholikar KB, Yang Z, Liu H. Identifying protein complexes with fuzzy machine learning model. Proteome Sci 2013:11. https://doi.org/10.1186/1477-5956-11-S1-S21.

[75] Deitz D, Harik I, Gesund H. One-way slabs reinforced with glass fiber reinforced polymer reinforcing bars. Spec Publ 1999;188:279–86.

[76] Kilpatrick A, Easden L. Shear capacity of GFRP reinforced high strength concrete slabs. Australas Conf Mech Struct Mater (18th 2004 Perth, Aust 2005:119–24.